CHAPTER - 9

STRUCTURAL AND MAGNETIC STUDIES OF HYDROXYAPATITE–ENCAPSULATED γ-Fe_2O_3 CORE-SHELL NANOPARTICLES

9.1 Introduction

Hydroxyapatite ($Ca_{10}(PO_4)_6(OH)_2$, HAP) has widely been used in biomedical and dental applications due to its similarity to main mineral components of hard tissues of human body such as bone, dental enamel and dentin and also its biocompatibility, bioactivity and low solubility in moist media [1-9]. In addition, it finds other prospective applications in various fields such as catalyst [10], ion exchanger [11], electrolyte for high temperature fuel cell [12], protein separation [13] and biosensors [14]. There has also been interested in the electrical properties of the material [15, 16]. Cobalt doped HAP films exhibited an excellent gas response and enhanced dielectric constant compared with pure HAP [17]. The dielectric studies of sodium and potassium ion exchanged HAP has conducted by Chavan *et al*. [18] revealed that the HAP nanomaterial not only supported the growth of apatite layer but also accelerated the growth onto itself.

Dielectric properties of iron oxide based nanomaterials were reported by Wang *et al*. [19] and they found the large dielectric constant and minimum dielectric loss in the oleic acid coated iron oxide NPs. Yang *et al*. [20] have observed that Fe_3O_4 particle at the nanoscale showed maximum magnetic permeability (M_r) due to their higher anisotropy energy. The efficient heterogeneous catalyst of combination of HAP and iron oxide NPs in the form of core-shell structure was reported by Mori *et al*. [21] and Zhang *et al*. [22] at 300 ºC calcined sample [21, 22]. They used these magnetic core-shell nanoparticles (CSNPs) as catalyst for the oxidation of various alcohols to carbonyl compounds and Knoevenagel condensation applications

respectively. These workers did not, however, measured the magnetic properties of this iron oxide core as a function of the temperature. For the electrical and chemical applications, strong sintering resistance and excellent durability under reaction atmosphere properties are desirable.

In this present study, biocompatible magnetic hydroxyapatite CSNPs were fabricated by cationic surfactant mediated co-precipitation process. Their structural and magnetic properties of synthesised particles were analysed after heat treatment at 650 ºC and also the influence of core-shell structure on the phase stability of γ-phase iron oxide at high temperature have been presented.

9.2 Experimental Section

9.2.1 Materials

$FeSO_4.7H_2O$ (Merck), $FeCl_3.6H_2O$ (Merck), Cetyl trimethyl ammonium bromide (CTAB) (Otto), H_3PO_4 (Central Drug House (CDH)) and $Ca(NO_3)_2.4H_2O$ (S. D. Fine Chemicals) were used for the synthesis of hydroxyapatite-encapsulated magnetic γ-Fe_2O_3 (γ-Fe_2O_3/HAP) CSNPs.

9.2.2 Method

For the synthesis of γ-Fe_2O_3/HAP CSNPs, $FeSO_4.7H_2O$ (1.85 mM) and $FeCl_3.6H_2O$ (3.7 mM) were dissolved in double distilled water (DDW) (30 ml), 10 ml of 25% NH_4OH solution was added drop-wise under vigorous stirring (3000 rpm). A black precipitate was observed instantly. After 15 min, 100 mL of $Ca(NO_3)_2.4H_2O$ (33.7 mM) and H_3PO_4 (20 mM) solutions whose pH were adjusted to 11 were added drop-wise to the obtained precipitate solution over 60 min under the mechanical stirring, respectively. The resulting brownish solution was heated at 90 ºC for 2 h. Finally, the mixture was cooled to room temperature and aged overnight without stirring. The obtained precipitate was filtered, washed repeatedly with DDW till

neutrality and air-dried at 100 ºC overnight. Finally, the dried samples were calcined at 650 ºC for 90 min giving a reddish-brown powder.

Thermo gravimetric analysis (TGA) was carried out from SII Nanotechnology Inc., Japan, EXSTAR6200 from the temperature range 35 ºC to 1000 ºC at a heating rate of 10 ºC min^{-1} in air. The phase purity and crystal structure of the synthesised samples were analysed by powder X-ray diffractometer (Rigaku Miniflex-II) at room temperature. The energy dispersive X-ray analysis (EDS) carried out by FEI Quanta 200 scanning electron microscope equipped with EDS. The micro-structural investigation of the CSNPs was carried out using transmission electron microscope (TEM) (TECHNAI G^2 TF20ST). Samples for TEM were prepared by placing a drop of colloidal acetone solution of the powder sample onto a carbon coated Cu grid and the grid was dried in air. Raman spectra of the samples were obtained at an excitation wavelength of 488 nm using a Lab-RAM HR 800 (Jobin Yvon) Raman spectrometer. Magnetic characterisation of the NPs was carried out using an ADE EV9 model vibrating sample magnetometer (VSM) by applying a maximum field of 20 kOe. 57Fe Mossbauer spectra were recorded using a 25 mCi 57Co(Rh) gamma ray source, the Mossbauer spectra were analysed using the PCMOS-II least-squares fitting program.

9.3 Results and Discussion

9.3.1 Thermo Gravimetric Analyses (TGA)

Thermogravimetric analyses (Figure 9.1a) of the bare γ-Fe_2O_3 NPs showed an initial mass loss of 3.9 weight percentage (wt%) due to removal of adsorbed water molecules followed by sharp peak at 440 ºC which is Curie point of the maghemite NPs. The Curie temperature (T_c) of bulk maghemite is 675 ºC.

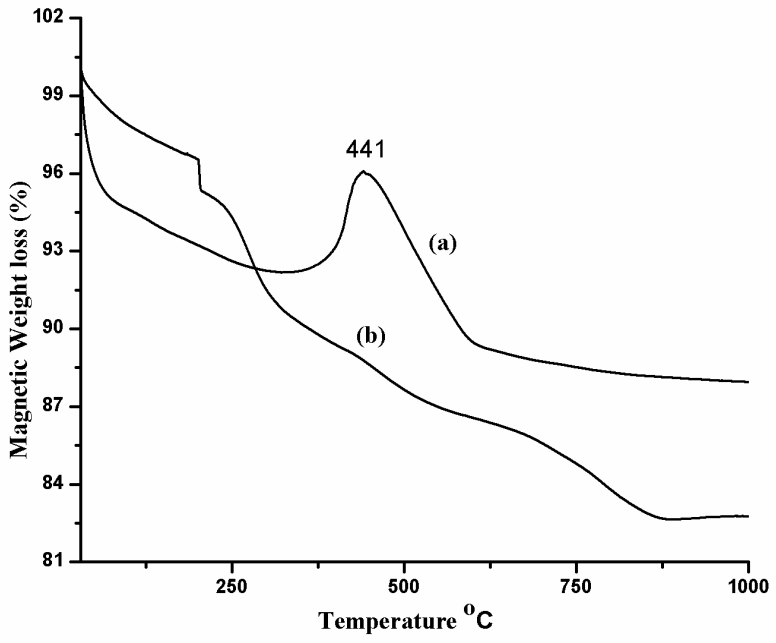

Figure 9.1 Thermogravimetric analyses of (a) bare γ-Fe_2O_3 NPs and (b) γ-Fe_2O_3/HAP CSNPs

Decreasing the T_c value for the maghemite NPs in the present case is associated with the nanoscale size effect. The magnetic weight loss of the γ-Fe_2O_3/HAP CSNPs (Figure 9.1b) showed a weight loss 1.2 wt% below the 200 ºC due to H_2O molecules removal followed by 4% mass loss corresponding to the nitrate molecule present in the HAP precursor material. The temperature range of 300 ºC - 600 ºC mass loss observed around 4.8 wt% due the decomposition and release of CTAB used in the reaction and above 600 ºC the minor mass loss due to decomposition of calcium deficient hydroxyapatite [23].

9.3.2 X-ray Diffraction Studies

The powder X-ray diffraction (XRD) patterns of the HAP, iron oxide and HAP coated γ-Fe_2O_3 are shown in Figure 9.2 (a-c). In the XRD pattern of iron oxide core NPs (Figure 9.2a) shows the existence of the major diffraction peaks of maghemite at 2θ values are 30.2°, 35.7°, 43.6°, 53.6°, 57.3° and 63.0° and the crystal planes are (220), (311), (400), (422), (511) and (440) respectively and these peaks data matched with JCPDS card number 89-5894. In the XRD pattern of the HAP NPs

(Figure 9.2b), the major peaks are obtained at 2θ = 25.9°, 32°, 33.2°, 34° and 49.5° corresponding to (002), (211), (300) and (202) hkl planes respectively. The nature and position of the above diffraction peaks are characteristics of hydroxyapatite phase as JCPDS card file number: 09-432.

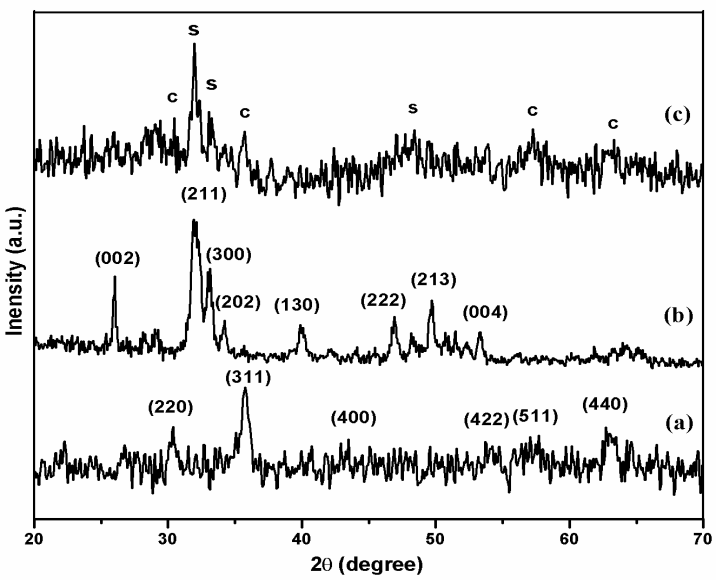

Figure 9.2 XRD patterns of the (a) γ-Fe_2O_3, (b) HAP and (c) γ-Fe_2O_3/HAP NPs

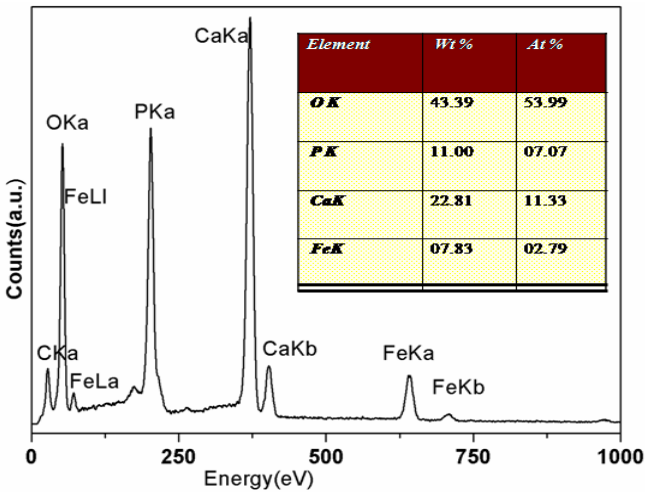

Figure 9.3 EDS profile and elemental percentage (inset Table) of γ-Fe_2O_3/HAP CSNPs

The HAP and γ-Fe_2O_3 diffraction patterns are observed in the γ-Fe_2O_3/HAP CSNPs systems are shown in Figure 9.2c. It exhibits clear peaks due to the HAP lattice along with γ-Fe_2O_3 phase at around 30.2°, 35.7°, 43.6° and 53.6° corresponding to the (220), (311), (400) and (422) reflection planes, respectively. Other iron oxide phases such as α-Fe_2O_3 and metallic bcc Fe NPs are apparently not seen. To further confirm the HAP coated iron oxide CSNPs, we undertook the energy dispersive X-ray spectrum (EDS) measurement (Figure 9.3) on the carbon tape was done. The results further revealed that the samples contain elements of calcium, phosphorous, iron and oxygen (inset Figure 9.3).

9.3.3 Raman Studies

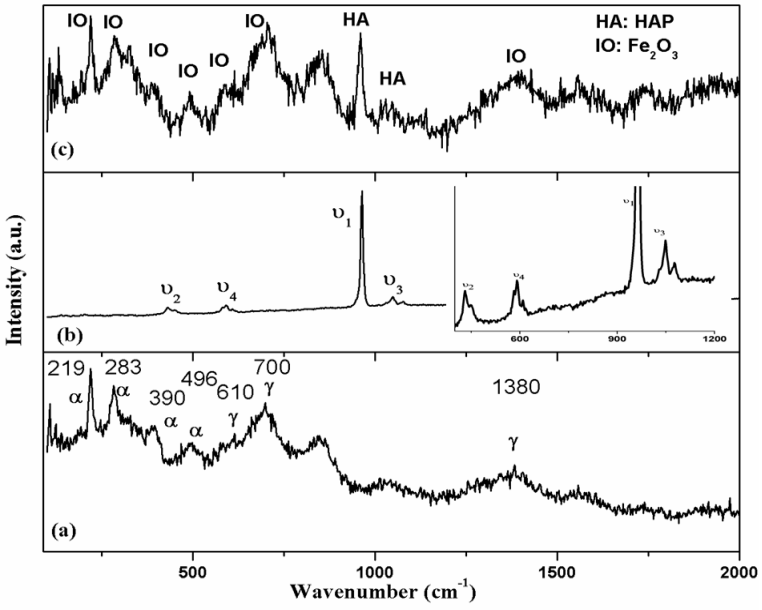

Figure 9.4 Raman spectra of (a) Fe_2O_3, (b) HAP and (c) γ-Fe_2O_3/HAP NPs. Inset of Figure 9.4b is the enlarge portion of HAP spectrum

Figure 9.4 shows the Raman spectra obtained for (a) Fe_2O_3, (b) HAP and (c) γ-Fe_2O_3/HAP CSNPs. The peaks seen at 219 cm^{-1} is assigned to the A_{1g} modes of iron oxide (Figure 9.4a). The remaining peaks at 283 and 610 cm^{-1} are assigned to the Eg modes. This indicates that the presence of hematite phase in the synthesised material.

However, the presence of 700 and 1380 cm^{-1} peak with the hematite seems that the samples contained the combination of hematite and maghemite phase [24-26]. The Raman spectrum for HAP is shown in the Figure 9.4b. Four distinguishable groups of spectral bands, the first group consist of two bands at ~ 432 and ~ 442 cm^{-1}. These bands correspond to the factor group splitting of the ν_2 bending vibrations of the PO_4^{3-} ion.

The bands present at ~ 579, 592 and 608 cm^{-1} belong to the ν_4 fundamental vibration mode and arise from the triply degenerate bending vibrations. The phosphate symmetric-stretch peak observed in the range of 962 cm^{-1} is characteristic for hydroxyapatite [27]. An increasing wave number for this peak indicates a more crystalline stoichiometry of hydroxyapatite particles. A very intense band obtained at 962 cm^{-1} arises from the symmetric stretching modes and is designated as ν_1 fundamental vibrational mode. The bands comprising the fourth group arise from the ν_3 fundamental vibrational modes and are due to the asymmetric stretching vibrations of the P–O bonds these bands are seen at ~ 1025, 1047 and 1087 cm^{-1}. The inset of Figure 9.4b is the enlarge portion of HAP spectrum and it clearly shows the four fundamental groups of HAP bands. In the case of CSNPs (Figure 9.4c), both core and shell material peaks are observed and also the peaks are broadened due to the thin layer of shell material in this 650 ºC heat treated CSNPs.

9.3.4 TEM Studies

The transmission electron micrographs obtained for γ-Fe_2O_3/HAP CSNPs are shown in Figure 9.5a and b. Figure 9.5a shows the particles are well dispersed and the average particle diameter is around 70 nm. The structure of these particles is in irregular shape. Figure 9.5b is the high magnification micrograph. It clearly displays the darker part of the magnetic core particle, which is encapsulated by the HAP shell

material, indicating the formation of core-shell structure. The multi core of magnetic NPs are encapsulated by the very thin layer of HAP shell material are observed and the agglomeration of particles are not observed. Coating of HAP on iron oxide particles prevents their interaction.

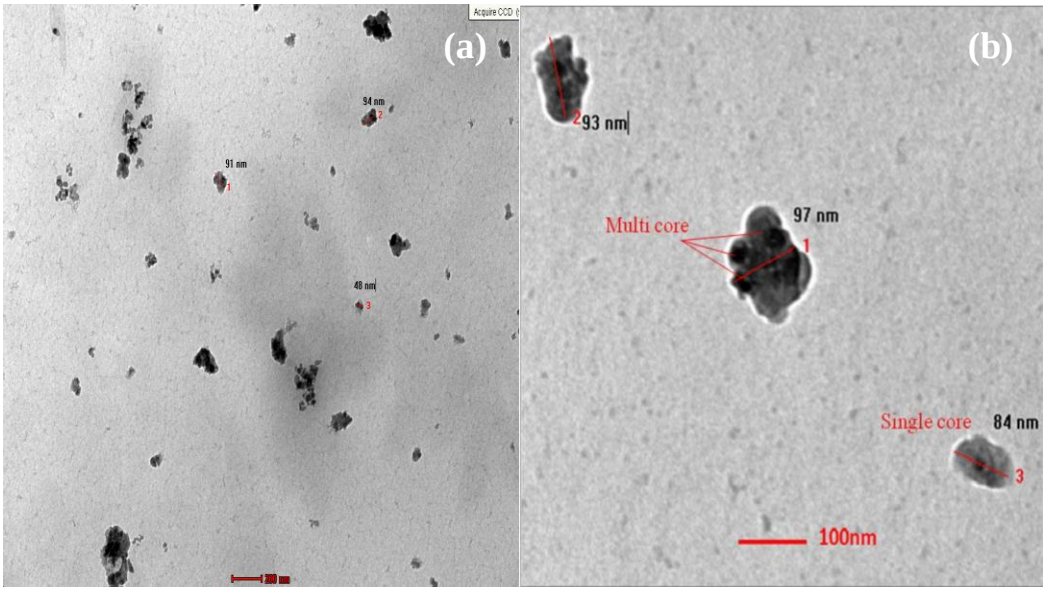

Figure 9.5 TEM micrographs of γ-Fe_2O_3/HAP CSNPs (a) lower magnification and (b) higher magnification

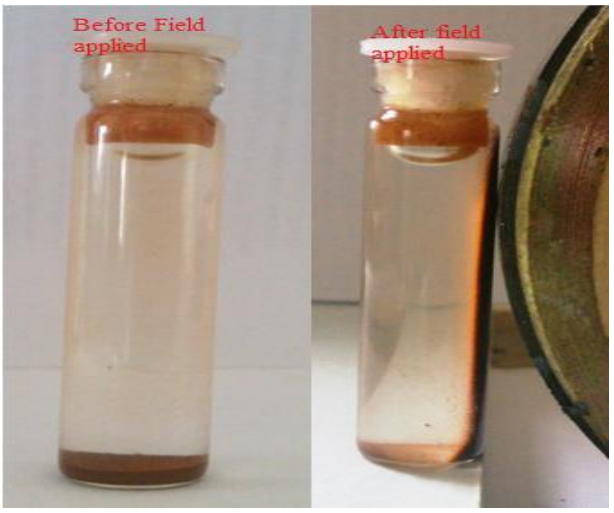

Figure 9.6 Magnetic property of γ-Fe_2O_3/HAP CSNPs with and without external magnetic field

The photographic images of Figure 9.6 shows the 650 ºC calcined γ-Fe_2O_3/HAP CSNPs in aqueous solution before and after the external magnetic field applied. When the magnetic field is applied, γ-Fe_2O_3/HAP CSNPs are completely aligned towards the external magnetic field. It confirms the magnetic phase of γ-Fe_2O_3 is retained by coating of HAP on the maghemite core after 650 ºC calcination of γ-Fe_2O_3/HAP CSNPs.

9.3.5 Vibrating Sample Magnetometer Studies

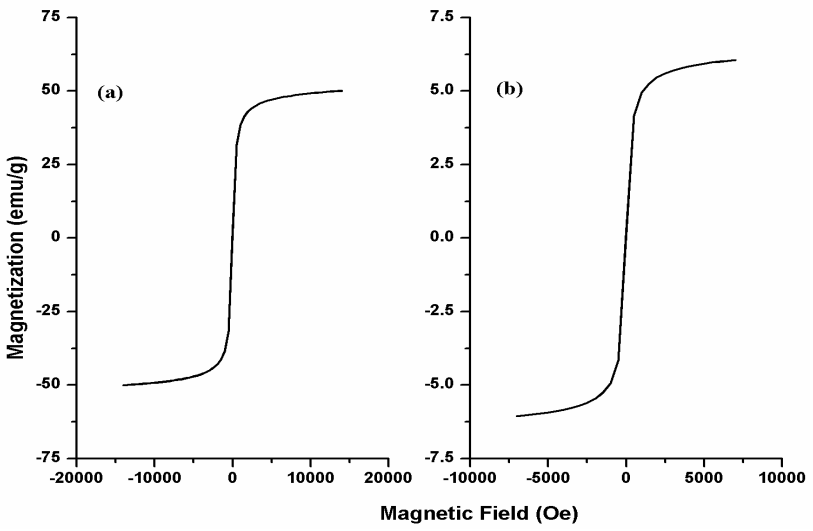

Figure 9.7 Room temperature magnetization of (a) γ-Fe_2O_3 and (b) γ-Fe_2O_3/HAP NPs

The hysteresis loops of γ-Fe_2O_3 (Figure 9.7a) and γ-Fe_2O_3/HAP CSNPs (Figure 9.7b) were measured at room temperature using vibrating sample magnetometer (VSM). The γ-Fe_2O_3 NPs show high magnetization around 50 emu/g and H_c value is 259 Oe. This large magnetization value indicates that the material having γ-Fe_2O_3 phase. A Raman spectrum of iron oxide contains hematite peak but hematite is antiferromagnetic in nature and its magnetization is negligible at 30 ºC. The presence of hematite phase in the Raman spectrum may be due to the heat-induced phase changes via the excitation source during the course of collecting a

Raman spectrum [28, 29]. As shown in Figure 9.6b, the γ-Fe_2O_3/HAP NPs shows rapid increase in magnetization with increasing applied magnetic field due to nanosize effect. Hysteresis curve shows the coercivity (H_c) nearly 225 Oe and the saturation magnetization (M_S) reached up to 6.0 emu/g. In the case of bare γ-Fe_2O_3 NPs (Figure 9.6a), the M_s of 50 emu/g was smaller than (76 emu/g) bulk γ-Fe_2O_3 at room temperature and it may be due to the nanoscale size effect. The magnetic γ-Fe_2O_3 phase of iron oxide is unstable above 250 ºC after that it would turn into nonmagnetic α-Fe_2O_3 phase but in the present case thermal stability of the γ-Fe_2O_3 core is increased by encapsulating the HAP shell on the γ-Fe_2O_3 core.

9.3.6 Mossbauer Studies

Figure 9.8 and 9.9 are the room temperature 57Fe Mossbauer spectra of the iron oxide and HAP coated iron oxide CSNPs. The original data was fitted into a singlet and two sextet patterns as summarized in Table 9.1. The Mossbauer spectra of maghemite and γ-Fe_2O_3/HAP CSNPs split into two sextets in an external magnetic field are observed. This is connected with ferromagnetic ordering of maghemite below the Curie temperature. Two observed sextets of lines correspond to Fe^{3+} cations position in the tetrahedral and the octahedral sites. The IS value of bare iron oxide is smaller than 0.5 mm/s (0.202 and 0.206 mm/s) suggested Fe^{2+} ion is absent and that the phase formed is pure maghemite (γ-Fe_2O_3).

For HAP coated iron oxide NPs, the values of isomer shift (IS), hyperfine field (Hf) and quadrupole splitting (QS) of two sextets are determined to be 0.219 and 0.078 mm/s, 481 and 426 KOe and 0.029 and 0.128 mm/s, respectively. Magnetic hyperfine fields of HAP coated iron oxide NPs increased from the bare iron oxide NPs. This indicates the crystalline phase of γ-Fe_2O_3 is sustained up to 650 ºC due to the coating of HAP on the γ-Fe_2O_3 particle surface. But in the case of IS value, 0.219

and 0.078 mm/s suggested mixed iron states of Fe^{2+} and Fe^{3+} ions present in this γ-Fe_2O_3/HAP CSNPs system.

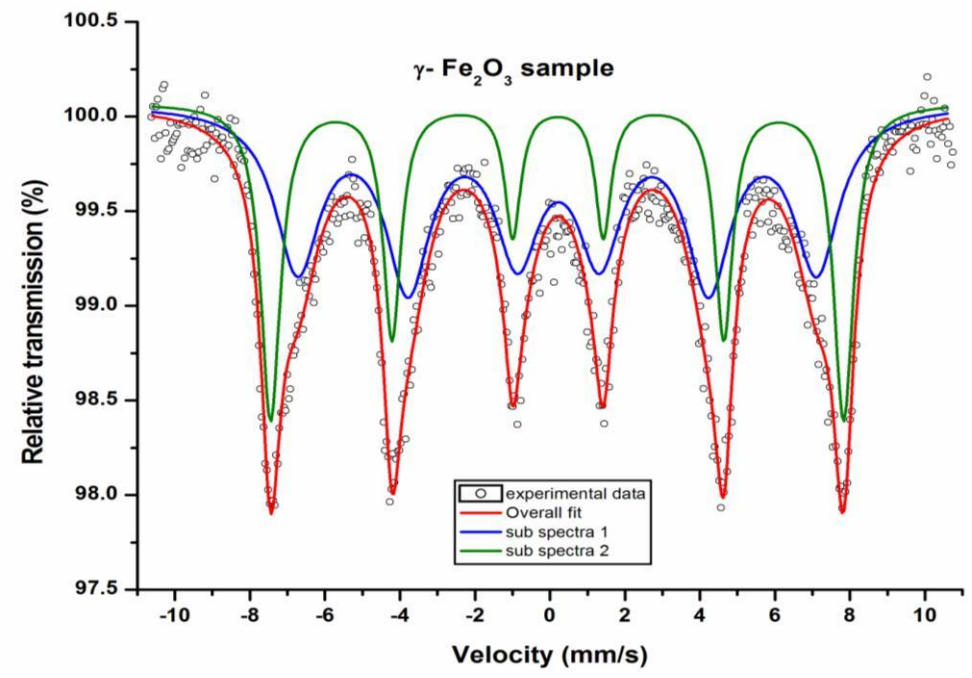

Figure 9.8 Room temperature 57Fe Mossbauer spectrum of iron oxide NPs

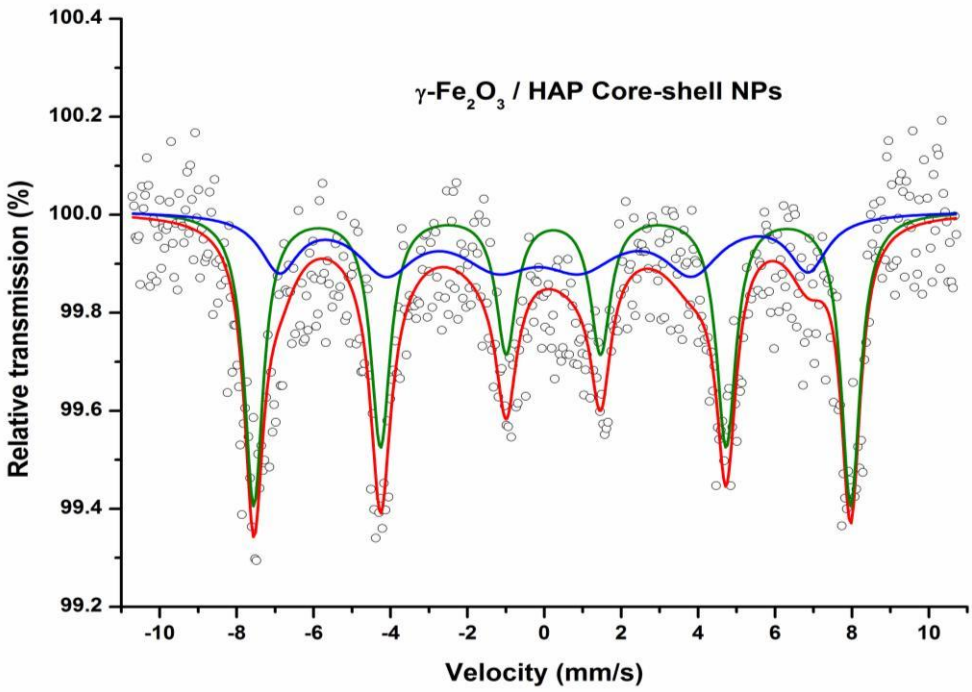

Figure 9.9 Room temperature 57Fe Mossbauer spectrum of γ-Fe_2O_3/HAP CSNPs

The VSM and Mossbauer results of HAP coated iron oxide CSNPs clearly indicate that the smaller portion of maghemite phase is transformed into hematite phase when subjected to the heat at 650 ºC. The room temperature hysteresis curve of the 650 ºC calcined CSNPs show the magnetic moment associated with the presence of thermally stable maghemite phase by the coating of HAP shell. During the heat treatment, possible of strong interaction between HAP and γ-Fe_2O_3 NPs surfaces and this interaction imposed by HAP can stabilize the crystal phase of γ-Fe_2O_3**.**

Table 9.1 Parameters obtained from Mossbauer studies for Fe_2O_3 and γ-Fe_2O_3/HAP CSNPs

Sample	**Sub Spectrum**	**Mossbauer Parameters**				
		H_{hf} (KOe)	**Quadrupole shift (ΔE_q) (mm/s)**	**Isomer Shift δ (mm/s)**	**Line width, WV (mm/s)**	**Relative Intensity (%)**
γ-Fe_2O_3	S1	474	0.023	0.202	0.64	56
	S2	429	0.031	0.206	1.20	44
γ-Fe_2O_3/HAP	S1	481	0.029	0.219	0.60	66
	S2	426	0.128	0.078	1.20	34

9.4 Conclusions

The HAP coated γ-Fe_2O_3 CSNPs are synthesised by simple co-precipitation method. Characterisation by means of physicochemical methods revealed that magnetic γ-Fe_2O_3 core was encapsulated by the HAP shell. The particles contained single and multi-core core-shell morphology and the average particle diameter is around 70 nm as calculated from the TEM studies. The hysteresis curve of HAP-γ-Fe_2O_3 nanoparticles showed the saturation magnetization (M_S) up to 6.0 emu/g. From the Mossbauer spectrum of HAP-γ-Fe_2O_3 NPs, coating of HAP over the iron oxide core gives the thermal stability of γ-phase Fe_2O_3 up to 650 ºC. This improved thermal stability is due to strong interaction between HAP and γ-Fe_2O_3 NP surfaces and the interaction imposed by HAP stabilized the crystal phase of γ-Fe_2O_3. The thermally stable HAP-γ-Fe_2O_3 CSNPs can be used for crystal-dependent catalysts, magnetic guided drug delivery and hyperthermia applications.

References

1. G. H. An, H. J. Wang, B. H. Kim, Y. G. Jeong and Y. H. Choa, Mat. Sci. Eng. A, 449-451 (2007) 821.
2. J. S. Cho and Y. C. Kang, J. Alloy. Compd. 464 (2008) 282.
3. J. S. Earl, D. J. Wood and S. J. Milne, J. Phys. Conf. Ser. 26 (2006) 268.
4. K. Lin, J. Chang, R. Cheng and M. Ruan, Mater. Lett. 61 (2007) 1683.
5. Y. Zhang, L. Zhou, D. Li, N. Xue, X. Xu and J. Li, Chem. Phys. Lett. 376 (2003) 493.
6. M. P. Ferraz, F. J. Monteiro and C. M. Manuel, J. Appl. Biomater. Biomech. 2 (2004) 74.
7. Q. Hu, B. Li, M. Wang and J. Shen, Biomaterials, 25 (2004)779.
8. C. G. Vazquez, C. P. Barba and N. Munguia, Rev. Mex. Fis. 51 (2005) 284.
9. F. Zhang, Z. H. Zhou, S. P. Yang, L. H. Mao, H. M.Chen and X. B. Yu, Mater. Lett. 59 (2005) 1422.
10. H. Zhong, R. Yuan, Y. Chai, W. Li and X. Zhong, Talanta, 85 (2011) 104.
11. A. J. Heeger, J. Phys. Chem. B, 105 (2001) 8475.
12. E. N. Konyushenko, J. Stejskal, M. Trchova, J. Hradil, J. Kovarova, J. Prokes, M. Cieslar, J. Y. Hwang, K. H. Chen and I. Sapurina, Polymer, 47 (2006) 5715.
13. C. Peng, J. Jin and G. Z. Chen, Electrochim. Acta, 53 (2007) 525.
14. J. Jiang and A. Kucernak, Electrochim. Acta, 47 (2002) 2381.
15. M. P. Mahabole, R. C. Aiyer, C. V. Ramakrishna, B. Sreedhar and R. S. Khairnar, Bull. Mater. Sci. 28 (2005) 535.
16. C. R. Bowen, J. Gittings, I.G. Turner, F. Baxter and J. B. Chaudhuri, Appl. Phys. Lett. 89 (2006) 132906.
17. M. P. Mahabole, R. U. Mene and R.S. Khairnar, Adv. Mat. Lett. 4 (2013) 46.
18. P. N. Chavan, M. M. Bahir, R. U. Mene, M. P. Mahabole and R. S. Khairnar, Mater. Sci. Eng. B, 168 (2010) 224.
19. T. Wang, W. Li, L. Luo and Y. Zhu, Appl. Phys. Lett. 102 (2013) 092904.
20. T. Yang, R. N. C. Brown, L. C. Kempel and P. Kofinas, J. Magn. Magn. Mater. 320 (2008) 2714.
21. K. Mori, S. Kanai, T. Hara, T. Mizugaki, K. Ebitani, K. Jitsukawa and K. Kaneda, Chem. Mater. 19 (2007) 1249.

22. Y. Zhang and C. Xia, Appl. Catal. A, 366 (2009)141.
23. Y. Li, W. Tjandra and K. C. Tam, Mater. Res. Bull. 43 (2008) 2318.
24. I. Chamritski and G. Burns, J. Phys. Chem. B, 109 (2005) 4965.
25. D. Bersani, P. P.Lottici and A. Montenero, J. Raman Spectrosc. 30 (1999) 355.
26. L. V. Gasparov, D. B. Tanner, D. B. Romero, H. Berger, G. Margaritondo and L. Forro, Phys. Rev. B: Condens. Matter Mater. Phys. 62 (2000) 7939.
27. D. E. Smeulders, M. A. Wilson and L. Armstrong, Ind. Eng. Chem. Res. 40 (2001) 10.
28. D. L. A. De Faria, S. V. Silva and M. T. De Oliveira, J. Raman Spectrosc. 28 (1997) 873.
29. M. Hanesch, Geophys. J. Int. 177 (2009) 941.

.